

Characterization of relativistic electron bunch duration and traveling wave structure phase velocity based on momentum spectra measurements

T. Vinatier^{✉,*}, R. W. Assmann,[†] F. Burkart[✉], H. Dinter, S. M. Jaster-Merz[✉], M. Kellermeier,
W. Kuropka[✉], F. Mayet[✉], and B. Stacey[✉]

Deutsches Elektronen-Synchrotron DESY, Notkestr. 85, 22607 Hamburg, Germany

C. Bruni

IJCLab, Université Paris Saclay, Bâtiment 100, 15 rue Georges Clémenceau, 91405 Orsay, France



(Received 25 July 2023; accepted 18 January 2024; published 14 February 2024)

The Accelerator Research Experiment at Sinbad (ARES) linac at DESY aims to generate and characterize ultrashort electron bunches (fs to sub-fs duration) with high momentum and arrival time stability for the purpose of applications related to accelerator research and development, e.g., development of advanced and compact diagnostics and accelerating structures, test of new accelerator components, medical applications studies, machine learning, etc. During its commissioning phase, the bunch duration characterization of the electron bunches generated at ARES has been performed with an rf-phasing technique relying on momentum spectra measurements, using only common accelerator elements (rf accelerating structures and magnetic spectrometers). The sensitivity of the method allowed highlighting different response times for Mo and Cs₂Te cathodes. The measured electron bunch duration in a wide range of machine parameters shows excellent agreement overall with the simulation predictions, thus demonstrating a very good understanding of the ARES operation on the bunch duration aspect. The importance of a precise *in situ* experimental determination of the phase velocity of the first traveling wave accelerating structure after the electron source, for which we propose a simple new beam-based method precise down to a variation of one part per ten thousand respective to the speed of light in vacuum, is emphasized for this purpose. A minimum bunch duration of 20 fs rms, resolution-limited by the space charge forces, is reported. This is, to the best of our knowledge, around 4 times shorter than what has been previously experimentally demonstrated based on rf-phasing techniques with a single rf structure. The present study constitutes a strong basis for future time characterization down to the sub-fs level at ARES, using dedicated X-band transverse deflecting structures.

DOI: [10.1103/PhysRevAccelBeams.27.022801](https://doi.org/10.1103/PhysRevAccelBeams.27.022801)

I. INTRODUCTION

A large number of scientific applications require ultrashort electron bunches with a duration typically below 100 fs rms and ideally even reaching the (sub)-fs level, e.g., ultrafast radiation pulse generation through free electron lasers [1] or wakefields [2], ultrafast imaging via diffraction and microscopy [3,4], ultrafast pulse radiolysis [5], etc. The ARES linac at DESY [6,7] aims to generate and characterize such bunches, with high momentum and time arrival stability, for the purpose of applications related to

accelerator research and development, e.g., development of advanced and compact diagnostics [8,9] and accelerating structures [10], test of new accelerator components, medical applications studies, etc. One of the main challenges to be faced toward this goal is to obtain a proper time characterization (duration, time profile, and arrival time jitter) of these bunches.

To reach the required resolution, several types of dedicated diagnostics are currently used worldwide. A (first) general type of method is based on electro-optical sampling of the electron bunch electromagnetic field with an ultrashort laser pulse [11]. This can be made single shot if a chirped laser pulse is used [12,13]. However, the resolution is by definition limited to the duration of the probing laser pulse, which is currently around a few tens of fs rms for commercially available lasers and therefore does not reach the single-digit fs to sub-fs level. Another general type of diagnostics is based on the bunch time profile reconstruction through a measurement of the frequency spectrum it emits in special conditions (e.g., Smith-Purcell

*Corresponding author: thomas.vinatier@desy.de

[†]Present address: GSI Helmholtzzentrum für Schwerionenforschung, Darmstadt, Germany.

Published by the American Physical Society under the terms of the [Creative Commons Attribution 4.0 International license](https://creativecommons.org/licenses/by/4.0/). Further distribution of this work must maintain attribution to the author(s) and the published article's title, journal citation, and DOI.

radiation [14], coherent transition radiation [15], etc.). These methods can reach a resolution on the single-digit femtosecond level for the bunch duration [16] but require assumptions on the shape of the electron bunch time profile to be able to reconstruct it and to deal with the fact that only part of the radiation spectrum is usually recorded [17]. A last general type of diagnostics is the transverse deflecting structure (TDS) [18]. By using a downstream dipole magnet with a dispersive direction perpendicular to the streaking direction of the TDS, the entire bunch longitudinal phase space (time vs momentum) can be recorded. Transverse deflecting structures working in the S-band frequency range are nowadays widely used with resolutions down to tens of fs rms [19], and transverse deflecting structures at higher frequencies, especially in the X-band range, are in development and allow reaching a (sub)-fs resolution [20]. Advanced streaking schemes are also currently under investigation to reach sub-fs resolutions, like the use of THz pulses [21] or methods aiming to combine the streaking provided by a laser modulator in one transverse direction with the streaking provided by a TDS on the orthogonal transverse direction [22].

The aforementioned techniques all require additional cost and a dedicated space to be implemented. Furthermore, the installation of an adequate environment (vacuum system, rf system, laser transport line, detectors, etc.) is also required for operation. Finally, for some of these techniques, the electron bunch has to interact in a controlled and synchronized way with an external radiation pulse (e.g., laser) introducing further complexity.

Several methods (thereafter named rf-phasing methods) exist to measure the bunch duration and time profile by using only common elements virtually present on all research electron accelerators (rf accelerating structures, spectrometer and imaging screens) and therefore do not require additional cost and space, e.g., zero-phasing technique [23], phase-scan methods [24–27], time-dependent transverse field components of TM_{01} mode [28], longitudinal phase-space tomography [29,30]. Despite not reaching the single-digit femtosecond resolution, these methods are still attractive to be used during the commissioning phase of an accelerator, before the implementation of dedicated diagnostics, but also on accelerators where no dedicated diagnostics are planned to be installed. This is, for example, the case on small accelerators for cost and/or space reasons or on the injectors for synchrotron light sources where the bunch duration is not a key parameter but can be of interest to be measured.

The primary diagnostics intended at ARES to diagnose the ultrashort electron bunches (see Table I) are two PolariX X-band transverse deflecting structures [31–33], which are the product of a collaboration between CERN, DESY, and PSI, for which the commissioning phase is expected to start in the first half of 2024. In addition to a

sub-fs resolution, it has the feature of a variable streaking direction, thus allowing advanced tomographic reconstruction of the bunch distribution [8,33].

In this paper, the commissioning phase leading to the first characterization of the duration of the electron bunches generated by the ARES linac at DESY (see Sec. II), which produced its first beam end of 2019 [6], is presented. The characterization of the bunch duration (see Sec. V) relies on the use of a phase-scan method [24,25], which is based on beam momentum spectra measurements (see Sec. III). A detailed comparison with the predictions from ASTRA simulations [34], a reference and well-benchmarked beam dynamics simulation code, is provided. An important requirement for this is a precise determination of the phase velocity of the first accelerating structure after the electron source, where the bunches are still not fully relativistic. To this aim, we propose a simple new method based on the measurement of the phase gap between momentum minima and maxima at the exit of this structure (see Sec. IV).

II. THE ARES LINAC AT DESY

The Accelerator Research Experiment at Sinbad (ARES) linac at DESY (see Fig. 1) is an approximately 45 m long linac operating in the S-band frequency range at 2.99792 GHz [6,7]. After the S-band gun, driven by a UV laser pulse at 257 nm, two 4.092 m long traveling wave accelerating structures (TWS1 and TWS2) operating in the $2\pi/3$ TM_{01} mode bring the electron bunches to their final momentum, around 155 MeV/c at maximum (gun + 2 TWS operated on crest). Several options are available to compress the electron bunches in time [35]: velocity bunching [36] in TWS1, magnetic compression in the bunch compressor [37], and a hybrid compression mode mixing velocity bunching and magnetic compression [38]. Two spectrometers (one after the gun and one at the end of the beamline) are available to diagnose the electron bunch momentum spectrum. The bunch charge is measured with a Faraday cup located before TWS1 unless otherwise stated in the paper. Multiple screens, steerers, and quadrupoles are located all along the beamline (not displayed in Fig. 1) for the purpose of beam transport, focusing, and diagnostics. The target bunch properties of the ARES linac are summarized in Table I. Some parameters are fixed for

TABLE I. Target electron bunch properties of the ARES linac at DESY.

Properties	Target value
Charge	0.01–200 pC
Momentum	20–155 MeV/c
Minimum momentum spread	0.01% rms
Bunch duration	Sub-fs to ≈ 10 fs rms
Transverse emittance (normalized)	$< 0.8 \pi$ mm mrad
Arrival time jitter	< 10 fs rms

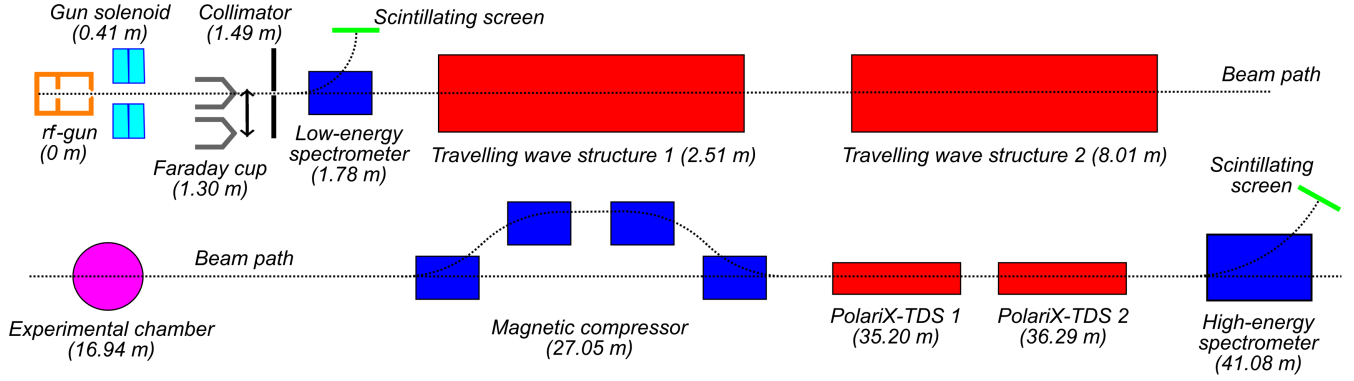


FIG. 1. Schematic layout of the ARES linac at DESY [6,7] with the relevant elements for the study presented in this paper. The positions are given relative to the rf-gun cathode plane and at the entrance of each element.

all the experimental results and simulations shown in the rest of the paper. They can be found in Table II.

Unless otherwise stated and when a single particle is considered, all the simulations presented in this paper include the effects of space-charge forces [39] on the electron bunch. They are calculated through the cylindrically symmetric algorithm implemented in the ASTRA software [34]. All the simulations presented in this paper start from the photocathode. The initial bunch distribution is generated using the generator software linked with ASTRA [34]. The isotropic model is used, where the emission angles of the electrons are isotropically distributed into a half-sphere pointing in the direction orthogonal to the photocathode plane. The width of the initial energy distribution of the electrons, the only free parameter in this model, has been adjusted such that the resulting transverse emittance at the rf-gun exit matches the one experimentally measured at ARES in [40]. We choose to neglect the variation of the accelerating field on the photocathode plane within the duration of the laser pulse driving it. This variation distorts the initial time profile of the electron bunch compared to the one of the laser pulse. The reason to neglect it here, is that the cathode laser pulse duration (175 fs rms) is much shorter than the period of the rf-gun accelerating field (≈ 333.565 ps). Finally, an exponential delay was added to the emission time of the electrons to simulate the response time of Cs₂Te photocathodes mounted in the ARES rf gun (see Secs. VA and VB).

It is important to note that there are no accelerating structures located downstream of the magnetic bunch compressor at ARES. It is therefore not possible to

perform a bunch duration measurement of the bunches coming out of it via rf-phasing methods. For this purpose, the PolariX transverse deflecting structures will be needed. The rf-phasing methods are, however, applicable to measure the bunches coming out of TWS1, eventually compressed in time via velocity bunching, since TWS2 is located right downstream.

III. THE PHASE-SCAN METHOD

The bunch duration measurements presented in Sec. V are performed with a phase-scan method [24,25], introduced in Sec. III A. This method has been selected rather than the other rf-phasing techniques because of its high flexibility and large range of applications.

Indeed, using the time-dependent transverse field components of the TM₀₁ mode in a TWS, as proposed in [28], is limited to the momenta of a few MeV/c. It is therefore not suited for ARES where the momentum is already ≥ 3.5 MeV/c after the gun and up to 80 MeV/c after TWS1. The phase-scan method is, on the opposite, also applicable at ultrarelativistic momenta.

The zero-phasing technique, as used in [23], has the advantage of maximizing the time resolution since the steepest slope of the rf accelerating field is used, thus maximizing the induced momentum spread. However, this comes with the drawback that the beam does not gain momentum in the rf structure or only in a very limited amount. This lower momentum results in stronger space-charge forces [39] during the beam transport downstream of the rf structure. This can influence the beam momentum spread and therefore the duration measured via the zero-phasing technique. Moreover, the zero-phasing technique requires assumptions to be placed on the input bunch momentum spread (if the two zero-crossing phases are used) and also on the input bunch time-momentum correlation (if only one zero-crossing phase is used). Typically, it is assumed that the input bunch momentum spread is negligible compared to the one imparted by the structure at the zero-crossing phase and eventually that the effect of the

TABLE II. Fixed operation parameters of the ARES linac at DESY.

Parameters	Values
Cathode laser rms duration	175 fs (Gaussian)
Cathode laser transverse profile	Uniform
TWS1 maximum average gradient	18.199 MV/m
TWS2 maximum average gradient	17.092 MV/m

time-momentum correlation can be neglected. Contrary to this, the phase-scan method requires only limited assumptions on the longitudinal phase space (see Sec. III A) and can be used with any phases of injection into the rf accelerating structure, also very close to on crest where the momentum gain is maximal.

A. The underlying model

The phase-scan method allows determining the statistical properties of the bunch longitudinal phase space (rms duration σ_t , rms momentum spread σ_p , and rms time/momentum correlation σ_{pt}) through the measurement of its momentum spread with a magnetic spectrometer for at least three conditions of operation of one or several upstream-located rf accelerating structures. The determined properties are then the ones at the entrance of the first accelerating structure which operation conditions are varied. It is analogous to the quadrupole scan technique in the transverse phase space [41].

It is in principle possible to vary either the field amplitude and/or the bunch injection phase into the accelerating structures. However, it is practically easier to vary the phase and only this option is considered in this paper. Also, only the case of a single traveling wave accelerating structure (TWS2) is considered in this paper.

In order to establish the analytical model on which the phase-scan method relies, several assumptions are made as follows:

(1) The space-charge forces effect on the measured momentum spread can be neglected all along the beam path from the entrance of the accelerating structure to the magnetic spectrometer.

(2) The effect on the momentum spread of the in- and out-coupling cells and of the leakage fields at the TWS entrance and exit can be neglected.

(3) The bunch is much shorter than the wavelength of the accelerating field so that its effect can be linearized whatever the injection phase.

(4) The bunch velocity can be assumed equal to c (speed of light in vacuum) so that the bunch duration and its phase slippage rate respective to the accelerating field are constant all along the structure (the latter being equal to zero if the field phase velocity is c).

The less these assumptions are fulfilled, the bigger the error on the reconstructed longitudinal bunch properties. On ARES, the typical charge (a few pC), momentum (35–80 MeV/c), and bunch duration (sub-ps rms) at the entrance of TWS2 are such that assumptions 3 and 4 are largely valid. To ensure the validity of assumption 4, we took care to experimentally use only injection phases into TWS2 leading to a momentum gain throughout the entire TWS2 so that no bunch momentum lower than 35 MeV/c is encountered. Practically, the minimal output bunch momentum used experimentally was around 65 MeV/c. Assumption 1 is also valid in a large range of parameters

but starts to become less and less valid for short bunches (typically below a few tens of fs rms). The validity of assumption 2 is assessed later in this section. It is important to note that assumption 4 is not fulfilled for TWS1 at ARES since the input bunch momentum is only around 3.8 MeV/c at maximum. As a result, the model derived in this section will only be applied with TWS2.

Under the aforementioned assumptions, the transport of the bunch longitudinal properties can be described by 2×2 matrices in the following way, assuming no coupling between the longitudinal and transverse planes:

$$\Sigma_f = M \Sigma_i M^T, \\ \text{with } \Sigma_\alpha = \begin{pmatrix} \sigma_{t_\alpha}^2 & \sigma_{pt_\alpha} \\ \sigma_{pt_\alpha} & \sigma_{p_\alpha}^2 \end{pmatrix} \text{ and } M = \begin{pmatrix} R_{55} & R_{56} \\ R_{65} & R_{66} \end{pmatrix}. \quad (1)$$

The subscripts i and f , respectively, refer to the entrance of the accelerating structure for which the operation condition is varied and the point where the momentum spread is measured. The superscript T refers to the transpose of a matrix. The matrix M is the longitudinal transfer matrix describing the beamline between i and f . The transport of the matrix Σ leads to the following equations:

$$\sigma_{t_f}^2 = R_{55}^2 \sigma_{t_i}^2 + 2R_{55}R_{56} \sigma_{pt_i} + R_{56}^2 \sigma_{p_i}^2, \quad (2)$$

$$\sigma_{p_f}^2 = R_{65}^2 \sigma_{t_i}^2 + 2R_{65}R_{66} \sigma_{pt_i} + R_{66}^2 \sigma_{p_i}^2. \quad (3)$$

Equation (2) is not experimentally useful since it would require measuring the bunch duration at the point f of the beamline to retrieve it at the point i . On the opposite, Eq. (3) is of interest since it links the bunch duration σ_{t_i} at the point i of the beamline to the momentum spread σ_{p_f} measured at the point f .

Under the aforementioned assumptions, the bunch momentum spread is invariant in a drift space or when focusing/transport magnets are used. Moreover, on ARES, there are no accelerating structures located downstream of the one used for the measurement (TWS2). This means that the momentum spread already has the value σ_{p_f} right at the exit of TWS2, or in other words, that only TWS2 contributes to the coefficient R_{65} and R_{66} in Eq. (3). The aforementioned assumptions also lead to $R_{66} = 1$ so that only R_{65} is relevant.

For a TWS, the on-axis longitudinal field component seen by an electron under the assumptions 3 and 4 can be written as

$$E_z(z) = E_m \cos \left(\frac{2\pi f(v_{ph} - c)}{v_{ph}c} z + \phi_0 \right), \quad (4)$$

where f is the TWS resonance frequency, E_m the maximal average gradient, z the position along the structure axis, c the speed of light in vacuum, and v_{ph} the phase velocity of the field in the TWS. ϕ_0 is the injection phase of the

electron bunch in the TWS (180° is the phase of maximum momentum gain rate for $v_{ph} = c$). At ARES, it is desired that v_{ph} is as close as possible to c , in order to minimize the phase slippage of the electron bunch. It has to be noted that a purely sinusoidal expression is used in Eq. (4), thus neglecting the spatial harmonics other than the fundamental in the TWS field. This is due to the fact that only the integrated effect throughout TWS2 is relevant for the phase-scan method, and these higher-order spatial harmonics provide no net momentum change when averaged over one period.

Defining $\xi(v_{ph}) = \pi f L (v_{ph} - c) / v_{ph} c$, the momentum p_f after TWS2 and R_{65} can be written as

$$p_f = p_i - \frac{e\widetilde{E}_m L}{c} \cos(\widetilde{\phi}_0), \quad (5)$$

$$R_{65} = \frac{2\pi f e \widetilde{E}_m L}{c} \sin(\widetilde{\phi}_0), \quad (6)$$

where L is the TWS length, e the fundamental electric charge, $\widetilde{E}_m = E_m \text{sinc}[\xi(v_{ph})]$, $\widetilde{\phi}_0 = \phi_0 + \xi(v_{ph})$, and $\text{sinc}(x)$ is the function equal to $\sin(x)/x$ for $x \neq 0$ and 1 for $x = 0$. It is noteworthy that $\xi(v_{ph})$ is half of the electron bunch phase slippage during its motion throughout TWS2.

One can see that by replacing E_m and ϕ_0 with the effective quantities \widetilde{E}_m and $\widetilde{\phi}_0$, including the effect of the bunch phase slippage respective to the TWS field, Eqs. (5) and (6) are written in the same way as the ones without phase slippage. This parameterization of the model with \widetilde{E}_m and $\widetilde{\phi}_0$ is convenient for practical application. Indeed, in practice, the TWS field amplitude in the model is adjusted to match the experimentally measured value of p_f . Doing so, it is not the actual TWS field amplitude E_m which is determined, but the effective TWS field amplitude \widetilde{E}_m which includes the effect of the bunch phase slippage. The values shown in Table II for TWS1 and 2 field amplitudes are therefore \widetilde{E}_m . Note that the actual value of E_m can be determined when v_{ph} is known through $E_m = \widetilde{E}_m / \text{sinc}[\xi(v_{ph})]$. Using $\widetilde{\phi}_0$ or ϕ_0 is strictly equivalent since $\xi(v_{ph})$ is a constant term, thus just implying a global translation of the injection phase scale. The origin of the injection phase scale is defined as the value maximizing the output bunch momentum. As a consequence, applying the phase-scan method at ARES with TWS2 under the assumptions made is therefore independent on its phase velocity and does not require its knowledge, while still including its effect.

All the measurements presented in Sec. V are performed by scanning the bunch injection phase $\widetilde{\phi}_0$ into TWS2 and the momentum spread σ_{p_f} is measured by the high-energy spectrometer (see Fig. 1). The reconstructed values of σ_{t_i} , $\sigma_{p_{t_i}}$, and σ_{p_i} from Eq. (3) are thus the ones at TWS2

entrance. This reconstruction requires an input of $n \geq 3$ values of σ_{p_f} measured for n values of $\widetilde{\phi}_0$ ($\equiv R_{65}$). A matrix system of the following form is obtained:

$$Y = AX, \quad \text{with} \quad Y = \begin{pmatrix} \sigma_{p_{f_1}}^2 \\ \vdots \\ \sigma_{p_{f_n}}^2 \end{pmatrix},$$

$$A = \begin{pmatrix} R_{65_1}^2 & 2R_{65_1} & 1 \\ \cdots & \cdots & \cdots \\ R_{65_n}^2 & 2R_{65_n} & 1 \end{pmatrix} \quad \text{and} \quad X = \begin{pmatrix} \sigma_{t_i}^2 \\ \sigma_{p_{t_i}} \\ \sigma_{p_i}^2 \end{pmatrix}. \quad (7)$$

This matrix system is inverted using a least-square algorithm to obtain the vector X and especially the bunch duration σ_{t_i} as follows:

$$X = (A^T A)^{-1} A^T Y. \quad (8)$$

To verify the validity of assumption 2, a comparison with an ASTRA simulation, where the effect of the in- and out-coupling cells and of the leakage fields at TWS2 entrance and exit is included, has been performed in ideal conditions. Namely, the space-charge forces were turned off after TWS2 entrance and it was ensured that the input distribution at TWS2 entrance had no coupling between the longitudinal and transverse planes. This enables us to isolate the combined influence of TWS2 in- and out-coupling cells and leakage fields on the phase-scan method accuracy. The bunch rms momentum spread at the high-energy spectrometer has been simulated as a function of the injection phase into TWS2 (see Fig. 2). Equation (8) has then been applied to the simulated dataset to reconstruct the bunch duration at TWS2 entrance. The reconstructed rms bunch duration (542.33 fs) is extremely close to the input one (542.24 fs), and the discrepancy is far below the typical error bars on experimental data and simulations (see Sec. V). The assumption 2 to neglect the effect of TWS2 in- and out-coupling cells and leakage fields is therefore valid. It is also confirmed that neglecting the spatial harmonics other than the fundamental in TWS2 field has a negligible effect, if any, on the phase-scan method accuracy since these harmonics are included in ASTRA.

In Fig. 2, an ASTRA simulation with the space-charge forces activated up to the end of the transport is also displayed. It is visible that the rms momentum spread differs only very marginally from the one simulated with space-charge forces turned off from TWS2 entrance. As a result, the reconstructed rms bunch duration (542.32 fs) is also extremely close to the input one (542.24 fs). The difference of the reconstructed bunch duration for the datasets with and without space-charge forces is negligible. This demonstrates the validity of assumption 1 for the conditions of Fig. 2, which are the ones for the reference

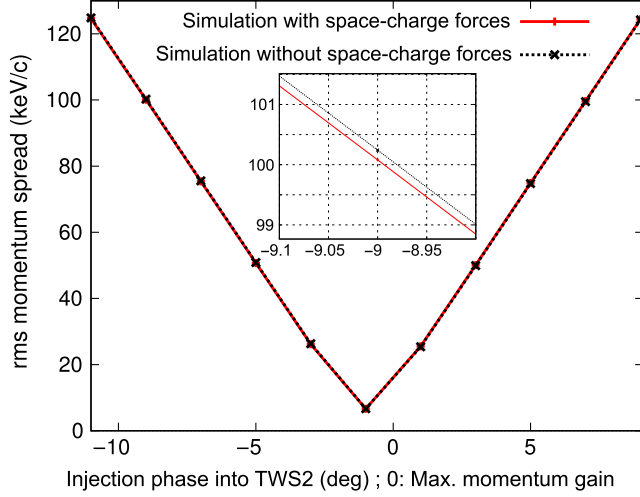


FIG. 2. ASTRA simulation of the bunch rms momentum spread at the high-energy spectrometer as a function of the injection phase into TWS2. The inset shows a close-up around one TWS2 phase. Conditions: 1 pC charge; 320 μm transverse diameter of laser pulse driving the gun; 74 MV/m gun peak accelerating field (rf gun at the phase maximizing the momentum \rightarrow 3.85 MeV/c output bunch); TWS1 at the phase maximizing the momentum \rightarrow 78.5 MeV/c output bunch; 542.24 fs rms bunch duration at TWS2 entrance; see Table II. Note: The simulation with or without space-charge forces refers only to the path into TWS2, the simulation up to TWS2 entrance is with space-charge forces.

working point at ARES where the three structures (gun, TWS1, and TWS2) are operated on crest.

One should note that Eq. (8) does not include any statistical errors (due to experimental jitters) on σ_{pf} and R_{65} . To address this, Eq. (8) is combined with a Monte Carlo algorithm [42]. The starting point is the measured experimental value of σ_{pf} , determined as the average of a small number (typically 10–30) of measurements, and its rms statistical error, determined as the standard deviation of these measurements. Then, a large number N (typically $N \geq 10^5$) of values of σ_{pf} is randomly generated following a Gaussian distribution with a standard deviation equal to the rms statistical error on σ_{pf} . Then, for each of these N values of σ_{pf} , one value of R_{65} is randomly drawn following a Gaussian distribution with a standard deviation equal to the rms statistical error on R_{65} (function of the experimental jitters on \widetilde{E}_m and $\widetilde{\phi}_0$). Applying Eq. (8) on each randomly generated doublet $(\sigma_{pf}; R_{65})$ generates a random set of N values for X . The final value for X is determined as the average of these N values and the error bar on it is their standard deviation.

B. Applicability criterion for the phase scan method

Qualitatively, a bunch duration threshold below which the phase-scan method cannot be applied exists. Namely, when the bunch becomes so short that the spectrometer is

unable to resolve at least three different values of σ_{pf} when scanning $\widetilde{\phi}_0$. Mathematically, this translates into the following theoretical applicability criterion for the phase-scan method:

$$\sigma_{pf_{\max}} - \sigma_{pf_{\min}} \geq 2R \left(\frac{p_{\max} + p_{\min}}{2} \right) = 2R \langle p \rangle \quad (9)$$

with $\sigma_{pf_{\max}}$ and $\sigma_{pf_{\min}}$ being, respectively, the maximal and minimal value of σ_{pf} , R being the relative resolution of the magnetic spectrometer (10^{-4} at ARES), and p_{\max} and p_{\min} , respectively, the maximal and minimal beam momentum in the range of phase between $\sigma_{pf_{\max}}$ and $\sigma_{pf_{\min}}$. We, therefore, approximate here the absolute spectrometer resolution (R times momentum) as equal to the one for the average beam momentum as a function of $\widetilde{\phi}_0$ in this range, $\langle p \rangle$. It is noteworthy that here, R does not refer to the spectrometer resolution for the measurement of an absolute value of σ_{pf} at a fixed $\widetilde{\phi}_0$, but to the resolution for the measurement of a variation of σ_{pf} between two values of $\widetilde{\phi}_0$.

It can be shown that $\sigma_{pf_{\max}}^2$ and $\sigma_{pf_{\min}}^2$ have the following expressions:

$$\sigma_{pf_{\max}}^2 = \alpha^2 \sigma_{ti}^2 + 2\alpha |\sigma_{pti}| + \sigma_{pi}^2, \quad (10)$$

$$\sigma_{pf_{\min}}^2 = \alpha^2 \sigma_{ti}^2 - 2\alpha |\sigma_{pti}| + \sigma_{pi}^2 \quad \text{if} \quad \left| \frac{\sigma_{pti}}{\alpha \sigma_{ti}^2} \right| \geq 1, \quad (11)$$

$$\sigma_{pf_{\min}}^2 = \sigma_{pi}^2 - \frac{\sigma_{pti}^2}{\sigma_{ti}^2} \quad \text{if} \quad \left| \frac{\sigma_{pti}}{\alpha \sigma_{ti}^2} \right| \leq 1 \quad (12)$$

with $\alpha = 2\pi f e \widetilde{E}_m L / c$. From Eqs. (9)–(12), the criterion for applicability of the phase-scan method can be verified for any input bunch and TWS2 properties.

It is noteworthy that the applicability criterion above is derived in ideal conditions and therefore gives the ultimate limit of the phase-scan method. It does not give the practical accuracy or resolution of the phase-scan method. Two important effects exist that prevent to measure a bunch duration as short as the applicability criterion would allow with the phase-scan method.

First, the criterion is defined such that only three values of σ_{pf} can be resolved, which is the very minimum to apply the phase-scan method. Under these conditions, the retrieved σ_{ti} is very sensitive to a single outlier value of σ_{pf} . Such an outlier value can, for example, be generated if an undetected time-limited and significant, namely much larger than the usual jitter, change of the experimental conditions happens (e.g., a jump of TWS2 accelerating gradient and/or phase). This unknown error will affect σ_{ti} , but it might not be reflected in its error bar (e.g., if the shot-to-shot jitter and therefore the error bar on σ_{pf} remains the

same before and after the TWS2 accelerating gradient and/or phase jump). The effect of such an outlier on σ_{t_i} can be significantly mitigated by recording more values (typically around 10) of σ_{p_f} as a function of the injection phase into TWS2 so that in practice $2R\langle p \rangle$ in Eq. (9) should be replaced by a higher number (typically $9R\langle p \rangle$ to be conservative).

Second, the duration of ultrashort bunches is not constant throughout TWS2 due to their initial time/momentum correlation at TWS2 entrance and the effect of the space-charge forces into TWS2. The space-charge forces also modify the value of σ_{p_f} between TWS2 entrance and the high-energy spectrometer. As a result, the retrieved value of σ_{t_i} is also modified, meaning in practice a worse resolution than the theoretical applicability criterion would allow. In other words, this means that the assumptions 1 and 4 of Sec. III A are not anymore fulfilled.

IV. INFLUENCE AND DETERMINATION OF THE TWS1 FIELD PHASE VELOCITY AS INPUT FOR THE SIMULATIONS

The primary goal of ARES is to generate ultrashort electron bunches. One of the schemes that can be applied to this aim is to compress the bunch via the velocity bunching process [36] in TWS1. This process is especially sensitive to the bunch input momentum (at TWS1 entrance) and to the field phase velocity v_{ph} in TWS1. These two parameters significantly influence the way the not ultrarelativistic electron bunch from the ARES gun (typically 3.5 to 4 MeV/c) is compressed in time via the velocity bunching process.

On the one hand, the input bunch momentum can be measured with an uncertainty better than a few percent with the low-energy spectrometer (see Fig. 1). On the other hand, to the best of our knowledge, there is no conventional method to precisely measure v_{ph} once a TWS is installed on an accelerator. Nevertheless, in order to be able to compare the bunch duration measured at TWS2 entrance via the phase-scan method with the prediction from ASTRA simulations, it is essential to precisely know v_{ph} for TWS1. Figure 3 illustrates this by comparing the TWS1 compression curve, namely the bunch duration after TWS1 as a function of the injection phase into it, simulated with ASTRA for several phase velocities. It shows that a deviation of $\pm 1\%$ respective to c (the design value for the TWS at ARES) leads to a significant distortion of the TWS1 compression curve, especially the injection phase leading to maximal compression is shifted by around $\pm 5^\circ$. The achieved minimal bunch duration remains, however, very similar for the different phase velocities.

For TWS2, the phase velocity has no significant influence on the electron bunch duration since it is already ultrarelativistic after TWS1 (at least 30 MeV/c and up to 79 MeV/c) and therefore almost frozen. In addition, as

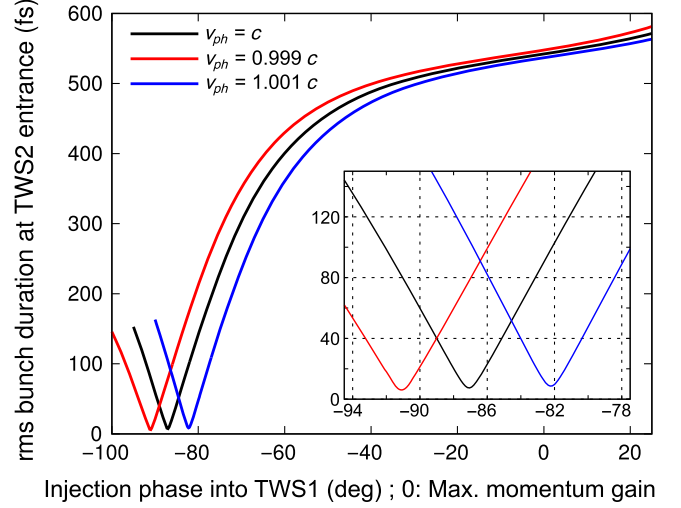


FIG. 3. Simulated rms bunch duration after TWS1 as a function of the injection phase into it for several phase velocities v_{ph} . The inset shows a close-up around the maximal compression. Conditions: 1 pC charge; 320 μm transverse diameter of laser pulse driving the gun; 74 MV/m gun peak accelerating field (rf gun at the phase maximizing the momentum \rightarrow 3.85 MeV/c output bunch); see Table II.

shown in Sec. III A, the knowledge of v_{ph} in TWS2 is not required to apply the phase-scan method.

To experimentally determine a TWS phase velocity, we propose a method taking advantage of a not ultrarelativistic input electron bunch, e.g., delivered by an rf gun. For such a bunch, the curve of the momentum after a TWS as a function of the injection phase exhibits a pattern with two maxima and a saddle point in between. The shape of this curve, all other parameters being fixed, strongly depends on the TWS phase velocity, as it is visible in Fig. 4(a). Several features of this curve can thus be used to experimentally determine the TWS phase velocity, e.g., the momentum value at the saddle point or the injection phase gap $\Delta\Phi$ between the maximum and the saddle point. Here we propose to use $\Delta\Phi$, because it is not affected by a potential miscalibration of the high-energy spectrometer.

The calibration curves $\Delta\Phi(v_{ph})$ for TWS1 and TWS2, generated through single particle and multiparticle ASTRA simulations with 10^4 macroparticles including space-charge forces, are, respectively, given in Figs. 4(b) and 4(c). The curves based on single particle simulations are almost superimposed with the ones based on multiparticle simulations, the discrepancy being at a maximum of 0.02° and therefore far below the experimental uncertainty on $\Delta\Phi$ (see Fig. 5). For visibility reason, only the quadratic fits for $\Delta\Phi(v_{ph})$ coming from single particle simulations are displayed on Figs. 4(b) and 4(c). The quadratic fit parameters of the simulated data points in Figs. 4(b) and 4(c) are shown in Table III.

Measurements of $\Delta\Phi$ have been performed at ARES for both TWS, the other TWS being switched off.

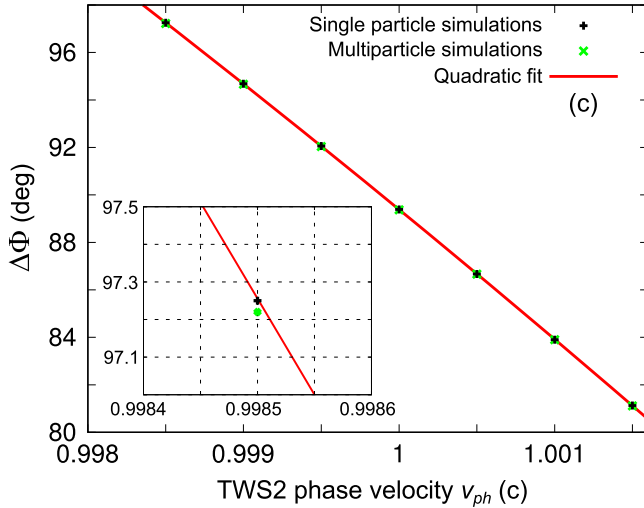
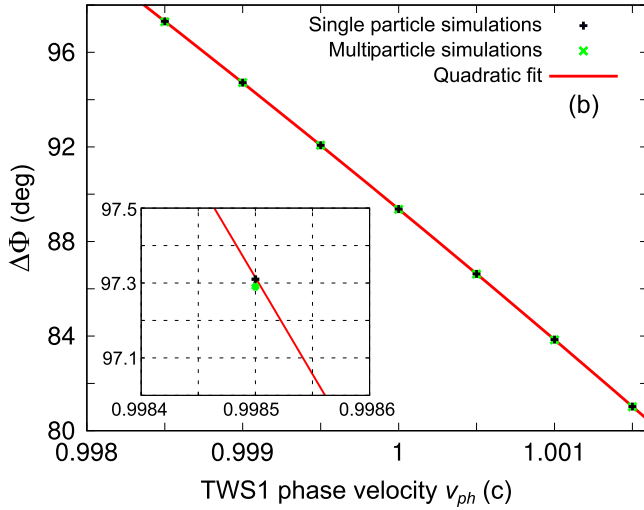
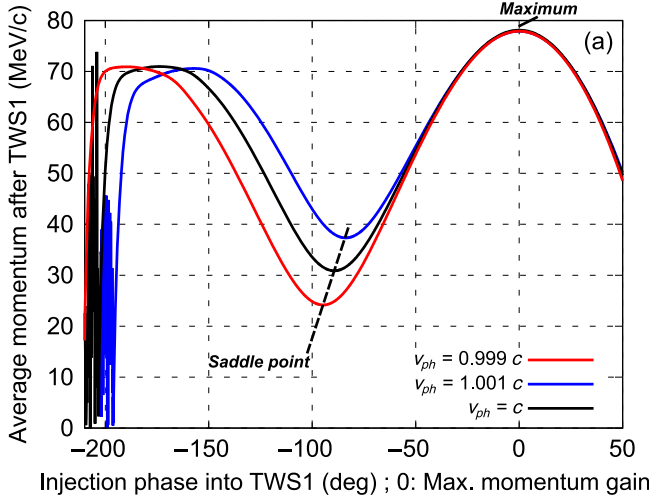


FIG. 4. (a) Simulated average momentum after TWS1 as a function of the injection phase into it for several phase velocities v_{ph} . Phase gap $\Delta\Phi$ between the maximum momentum and saddle point as a function of v_{ph} for TWS1 (b) and TWS2 (c). Conditions: Single particle and multiparticle simulations; see caption of Fig. 5; see Table II.

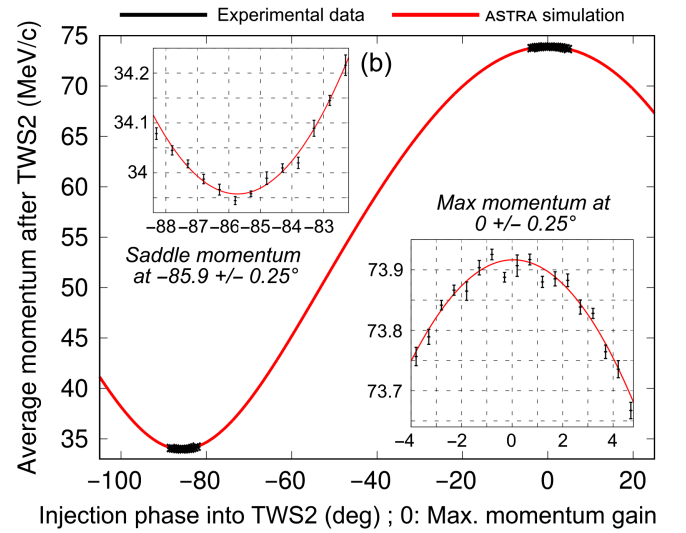
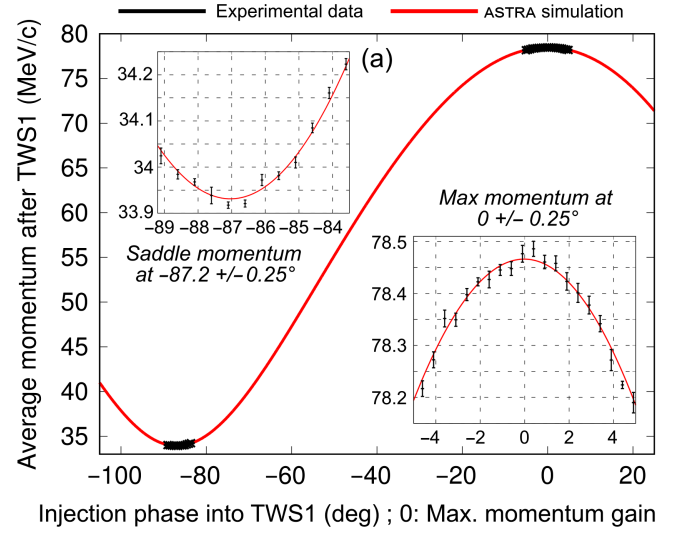


FIG. 5. Raw data for experimental determination of TWS1 (a) and TWS2 (b) phase velocities (average momentum as a function of injection phase). The insets show close-up around the maximum and saddle momentum phase ranges. Conditions: Mo cathode; 0.9 pC (a) and 0.25 pC (b) charge; 320 μm transverse diameter of laser pulse driving the gun; 74 MV/m gun peak accelerating field (RF-gun at the phase maximizing the momentum \rightarrow 3.85 MeV/c output particle); TWS2 off (a); TWS1 off (b); See Table II.

Figure 5 shows the raw data used to determine $\Delta\Phi$ (average momentum vs injection phase). A smaller charge has been used for the measurement with TWS2, in order to ease the transport of the 3.85 MeV/c bunch in the 8.01 m drift to its entrance (against 2.51 m for TWS1), since TWS1 is turned off. The values of $\Delta\Phi$ displayed in Fig. 5 have been determined through two parabolic fits of the experimental data, one around the maximum and one around the saddle point, optimized via a Monte Carlo algorithm [42] based on the experimental error bars.

Using the calibrations shown in Table III, the values of v_{ph} for TWS1 and TWS2 have been computed from the

TABLE III. Calibration curves $v_{ph}(\Delta\Phi)$ for TWS1 and TWS2 based on single particle and multiparticle (10^4 macroparticles including space-charge forces) ASTRA simulations. The quadratic expression $v_{ph}(\Delta\Phi) = a\Delta\Phi^2 + b\Delta\Phi + d$, with v_{ph} in units of c and $\Delta\Phi$ in degrees, is used for the fit. Conditions: See captions of Figs. 4 and 5.

Case	a	b	d
TWS1 (single particle)	-5.700×10^{-7}	-8.234×10^{-5}	1.01191
TWS1 (multiparticle)	-5.781×10^{-7}	-8.083×10^{-5}	1.01184
TWS2 (single particle)	-5.749×10^{-7}	-8.327×10^{-5}	1.01204
TWS2 (multiparticle)	-5.847×10^{-7}	-8.163×10^{-5}	1.01197

experimentally measured values of $\Delta\Phi$. The results are shown in Table IV, where the results based on the calibrations obtained with single particle and multiparticle simulations are compared. Using the error bars on $\Delta\Phi$ from Fig. 5 ($\pm 0.5^\circ$), the error bars on v_{ph} have been computed to $\pm 0.000091 c$ for all the cases shown in Table IV. The error bars on $\Delta\Phi$ and v_{ph} include the effect of all the machine jitters having an influence. These machine jitters are mainly the phase and amplitude jitters of the accelerating structures (rf gun and TWS), the timing jitter of the cathode laser, and the additional jitters influencing the momentum measurement with the high-energy spectrometer (pointing jitter and jitter of the current driving the dipole magnet). In Fig. 5, ASTRA simulations, where the experimentally determined v_{ph} are used, are also shown for comparison.

One can see in Table IV that the values of v_{ph} extracted using the calibration curves based on single particle and multiparticle ASTRA simulations are extremely close to each other, for a given TWS, and far below the experimental error bar coming from the determination of $\Delta\Phi$. This demonstrates that for the conditions used at ARES, it is fully valid to use only single particle simulations to establish the calibration curve $\Delta\Phi(v_{ph})$. This leads to a significant gain of time, a few tens of minutes with single particle simulations against several days with multiparticle simulations since $\Delta\Phi$ has to be determined with high precision (0.02° in our case) for this purpose. It is also noteworthy that despite their different average gradient

TABLE IV. Phase velocities v_{ph} obtained for TWS1 and TWS2 at ARES through the calibrations shown in Table III. The results based on the calibrations obtained with single particle and multiparticle (10^4 macroparticles including space-charge forces) ASTRA simulations are compared.

Case	$\Delta\Phi$	v_{ph}
TWS1 (single particle)	87.2°	$1.000396 c$
TWS1 (multiparticle)	87.2°	$1.000396 c$
TWS2 (single particle)	85.9°	$1.000645 c$
TWS2 (multiparticle)	85.9°	$1.000644 c$

(≈ 1.1 MV/m), using the calibration curve for TWS1 to determine $v_{ph}(\text{TWS2})$ or vice versa would lead to a limited error. In fact, it would lead to $v_{ph}(\text{TWS2}) = 1.000631 c$ instead of $1.000644 c$, which is well below the experimental error bar.

A last important step is to quantify the effect of the typical uncertainty on the input bunch momentum at ARES on the measurement procedure described above. This is required because a not ultrarelativistic input bunch momentum also has a significant influence on the phase slippage in the TWS. An error in its determination therefore comes with an error in the determination of the calibration curve of Table III, since it is determined for a fixed value of the input bunch momentum, and subsequently on the determination of v_{ph} . To this aim, it has been simulated which error on the input bunch momentum (measured at 3.85 MeV/c) would be necessary to retrieve the same $\Delta\Phi$ than in Fig. 5 assuming $v_{ph}(\text{TWS1}) = c$ (the design value). As for Fig. 4, the results coming from single particle and multiparticle ASTRA simulations have been compared.

Figure 6 shows that an input bunch momentum of around 3.12 MeV/c, translating into an error of 23.4%, would be required to reach the measured $\Delta\Phi = 87.2^\circ$ if $v_{ph}(\text{TWS1})$ was equal to c . This is much higher than the uncertainty on the bunch momentum measurement at ARES, which is typically of a few percent at maximum, corresponding to around 0.1 MeV/c. Besides, this maximal error of 0.1 MeV/c translates into an error of around 0.25° on

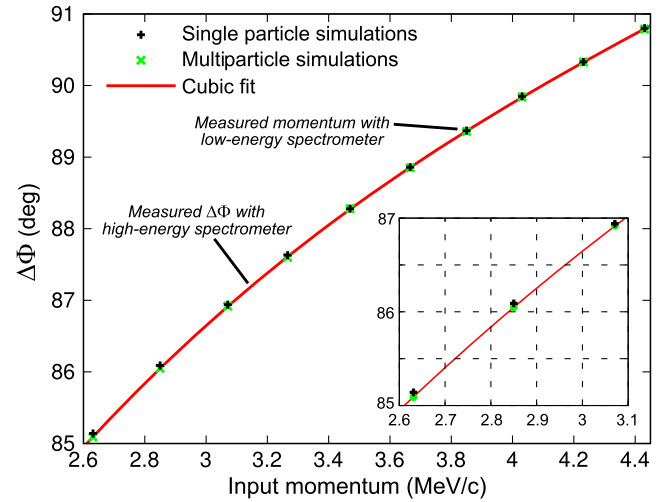


FIG. 6. Phase gap $\Delta\Phi$ between the maximum momentum and saddle point at the exit of TWS1 as a function of the input bunch momentum. Conditions: Single particle and multiparticle (10^4 macroparticles including space-charge forces) ASTRA simulations; rf gun at the phase maximizing the momentum (field amplitude is varied to change the bunch momentum); $v_{ph}(\text{TWS1})$ assumed equal to c (the design value); see caption of Fig. 5(a) and Table II.

$\Delta\Phi$, which is significantly lower than the uncertainty on the experimental measurement of $\Delta\Phi$ due to machine jitters (0.5°), which has been previously determined by parabolic fits of the experimental data of Fig. 5 combined with a Monte Carlo algorithm. This demonstrates that the uncertainty on the input bunch momentum would only marginally modify the determined value of v_{ph} . To take this into account, its contribution to the uncertainty on $\Delta\Phi$ (0.25°) is quadratically added to the one from the machine jitters (0.5°), resulting in an overall uncertainty of 0.56° . This increases the uncertainty on v_{ph} from $0.000091c$ to $0.00010c$. For the simulations performed in this paper, we considered $v_{ph}(\text{TWS1}) = 1.00040c \pm 0.00010c$ and $v_{ph}(\text{TWS2}) = 1.00064c \pm 0.00010c$.

A slight trend can be noticed in Fig. 6. Namely, the discrepancy in $\Delta\Phi$ between the single particle and multi-particle ASTRA simulations tends to increase when the input bunch momentum decreases, up to 0.06° discrepancy at 2.63 MeV/c . This is higher than the discrepancy in Fig. 4, where a 3.85 MeV/c input momentum is used, which is at a maximum of 0.02° and therefore within the statistical noise ($\Delta\Phi$ being simulated with 0.02° precision in our study). These 0.06° remains well below the experimental uncertainty on $\Delta\Phi$ and therefore of limited relevance on ARES. However, this is an indication that if a much lower input bunch momentum is used, e.g., from a dc gun, the use of single particle simulations to determine $\Delta\Phi(v_{ph})$ might not be valid anymore and has to be tested carefully.

As mentioned before, the knowledge of $v_{ph}(\text{TWS2})$ is not required for the bunch duration measurement method presented in Sec. III A. It is, however, of interest to be measured, for comparison with $v_{ph}(\text{TWS1})$. Indeed, although the two TWS at ARES are based on the same design, it is visible that their v_{ph} are different, namely they do not overlap within the error bars. It shows that v_{ph} is specific to a single TWS when installed on an accelerator and that it has to be characterized separately for each of them. The method described in this section is suited for this and can be applied to any accelerator, with a precision down to a variation of one part per ten thousand of v_{ph} respective to c . The condition for application is that a not ultrarelativistic beam (typically $\leq 5 \text{ MeV/c}$) of precisely known momentum (uncertainty better than a few percent) can be delivered at the entrance of the TWS and a downstream momentum measurement is available. This method is of general interest for facilities aiming to produce short bunches using the velocity bunching process since v_{ph} has a major influence on it.

V. BUNCH DURATION MEASUREMENTS AT ARES USING THE PHASE-SCAN METHOD

A. Comparison of Mo cathode and Cs_2Te cathode

Two different types of cathodes are used as electron source in the ARES rf gun: Mo (metal) and Cs_2Te

(semiconductor). From the literature, it is known that Cs_2Te has a longer response time than Mo. Direct measurements of Cs_2Te cathode response times in rf guns have been performed using electron microbunches with adjustable time separation generated by laser interferometry [43,44]. A value around 370 fs has been measured using a zero-phasing technique as diagnostic on the LUCX facility at KEK [43], and more recently, values between 180 and 250 fs (for different cathodes) have been measured on the PITZ facility at DESY using a TDS [44].

The cathode laser used at ARES to drive the rf gun has a duration of 175 fs rms , which is slightly shorter than the shortest Cs_2Te response time reported in the literature (180 fs) and is expected to be significantly longer than the Mo response time. Experimental measurements of the bunch duration at ARES in exactly the same conditions for a Mo and a Cs_2Te cathode should therefore give different values, due to the different response times. A comparison with ASTRA simulations with a varying response time can then be used to estimate the response time of the Cs_2Te cathode mounted in the ARES rf gun. This estimated value will then be used later in the paper when comparing experimental measurements made with Cs_2Te cathodes with simulations.

A bunch duration measurement using the phase-scan method has been performed in identical conditions for a Mo and a Cs_2Te cathode. The raw data used for the reconstruction of the bunch duration (momentum spread against injection phase into TWS2) are shown in Fig. 7. It is visible that the momentum spread for the Cs_2Te cathode increases faster with phase than for the Mo cathode when

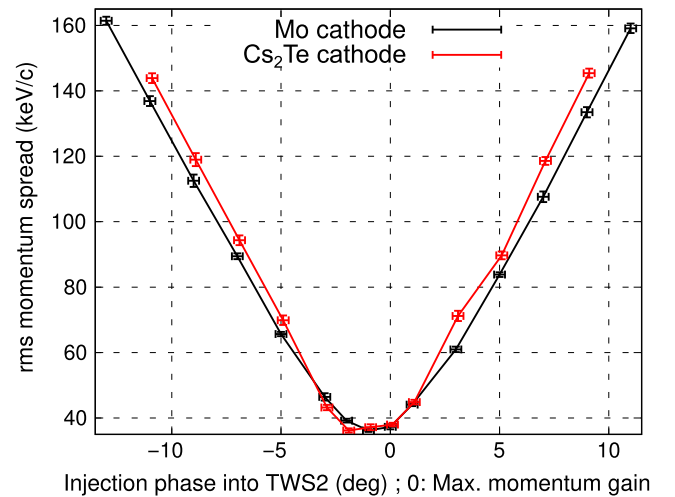


FIG. 7. Raw data for bunch duration determination at TWS2 entrance (rms momentum spread as a function of injection phase) for Mo and Cs_2Te cathodes in identical conditions. Conditions: $(1.07 \pm 0.015) \text{ pC}$ charge; $320 \mu\text{m}$ transverse diameter of laser pulse driving the gun; 70.6 MV/m gun peak accelerating field (3.69 MeV/c output momentum); injection phases into rf gun and TWS1 adjusted to maximize the momentum; see Table II.

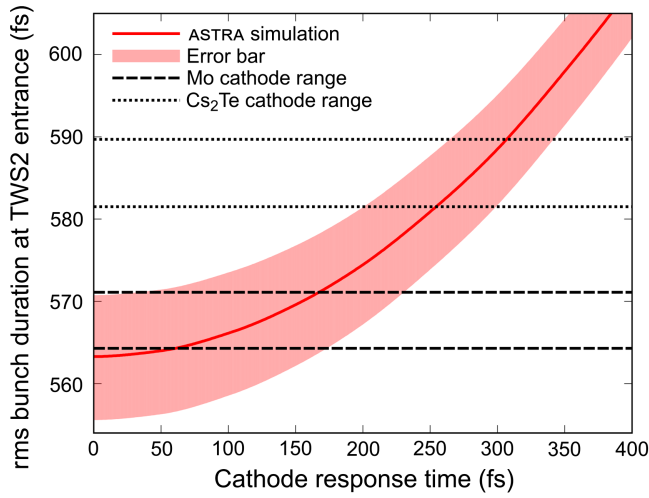


FIG. 8. rms bunch duration at TWS2 entrance as a function of the cathode response time simulated by ASTRA compared with the experimental values measured for a Mo and a Cs_2Te cathode with their uncertainty ranges. The error bar on the ASTRA simulation has been computed by including the jitter on the bunch charge, an uncertainty of ± 0.25 A on the current injected into the focusing solenoid located after the rf gun, and the uncertainty on TWS1 phase velocity. Conditions: See Fig. 7 caption.

moving away from the minimum, which is due to a longer bunch duration at TWS2 entrance resulting from the Cs_2Te longer response time. An analysis of the data in Fig. 7 with the model of Sec. III A gives at TWS2 entrance a bunch duration of (567.7 ± 3.4) fs rms for the Mo cathode and (585.6 ± 4.1) fs rms for the Cs_2Te cathode.

A comparison of the aforementioned bunch durations with those obtained in ASTRA simulations as a function of the cathode response time is shown in Fig. 8. From Fig. 8, it is visible that the bunch duration measured for the Mo cathode is compatible with a very short response time (we will assume it equal to 0 in the rest of the paper), while the one measured for the Cs_2Te cathode points toward a higher response time in the range between 200 and 300 fs. A detailed Monte Carlo analysis of the overlap between the simulation curve and the range for the experimentally measured duration gives an estimated response time of (271.4 ± 32.4) fs (at one standard deviation) for the Cs_2Te cathode. This estimated value is within the range coming from direct experimental measurements [43,44] and is therefore compatible with them. It will be used for comparison with simulations in Sec. V B when a Cs_2Te cathode is mounted in the ARES rf gun.

B. Systematic bunch duration measurements with the phase-scan method at ARES

The bunch duration at TWS2 entrance has been measured at ARES as a function of three parameters having a significant influence on it: the rf-gun field amplitude [Fig. 9(a)], the bunch charge [Fig. 9(b)], and the injection

phase into TWS1 [Fig. 9(c)]. Aside of each bunch duration curve, a selection (for visibility reason) of the raw data used for the measurement (rms momentum spread as a function of the injection phase into TWS2) is also displayed.

At the time when the data for Fig. 9(c) were acquired, a large amount of dark current through field emission [45] was generated in the rf gun, mainly coming from its backplane and the cathode. To reduce it, a 1 mm diameter collimator was used in the gun region, before TWS1 (see Fig. 1). At the time when the data for Fig. 9(b) were acquired, a similarly high level of dark current was present. To reduce it without using the collimator, which would also cut the bunch charge, we reduced the rf-gun gradient from 69.5 to 64.9 MV/m. At a later point, a CO_2 cleaning of the ARES rf gun was performed, greatly reducing the level of generated dark current. This allowed increasing the gun gradient up to 74 MV/m, without introducing significant disturbances in the measurement by the dark current. Figure 9(a) was then completed with the two highest gradient points and the measurements of the TWS phase velocities presented in Sec. IV were performed, the latter being independent of the gun gradient.

The experimental results are compared with the prediction from ASTRA simulations, in order to evaluate our understanding of the ARES operation on the aspect of bunch duration. Note that for this purpose, the TWS1 phase velocity determined in Sec. IV is used. For Figs. 9(a)–9(c), the error bar on the ASTRA simulation includes the jitter on the bunch charge, an uncertainty of ± 0.25 A on the current injected into the focusing solenoid located after the rf gun and the uncertainty on the TWS1 phase velocity. For Fig. 9(c), since a Cs_2Te cathode and a 1 mm diameter collimator were used, the uncertainties on the cathode response time and the bunch charge after the collimator (measured with a resonator [46]) are also included.

The experimental results in Fig. 9 are in very good agreement with the ASTRA simulations, with almost all the points matching within the error bars. This demonstrates a very good understanding of the ARES operation on the bunch duration aspect for a large range of parameters. The preparatory experimental determination of the TWS1 phase velocity (Sec. IV) is especially important to compare Fig. 9(c) with ASTRA simulations. This is illustrated by Fig. 10, where the experimental data of Fig. 9(c) are compared with ASTRA simulations where a TWS1 phase velocity equal to c (the design value) is used instead of the measured $1.00040c$ used in Fig. 9(c). It is clearly visible that, even for this small change of the phase velocity, a significant discrepancy between the ASTRA simulation and the experimental data, not covered by the error bars, would appear when approaching and overcoming the TWS1 phase for maximal compression.

To quantify the better agreement between the experimentally measured bunch duration and the simulated one when the measured $v_{ph}(\text{TWS1})$ ($1.00040c$) is used in

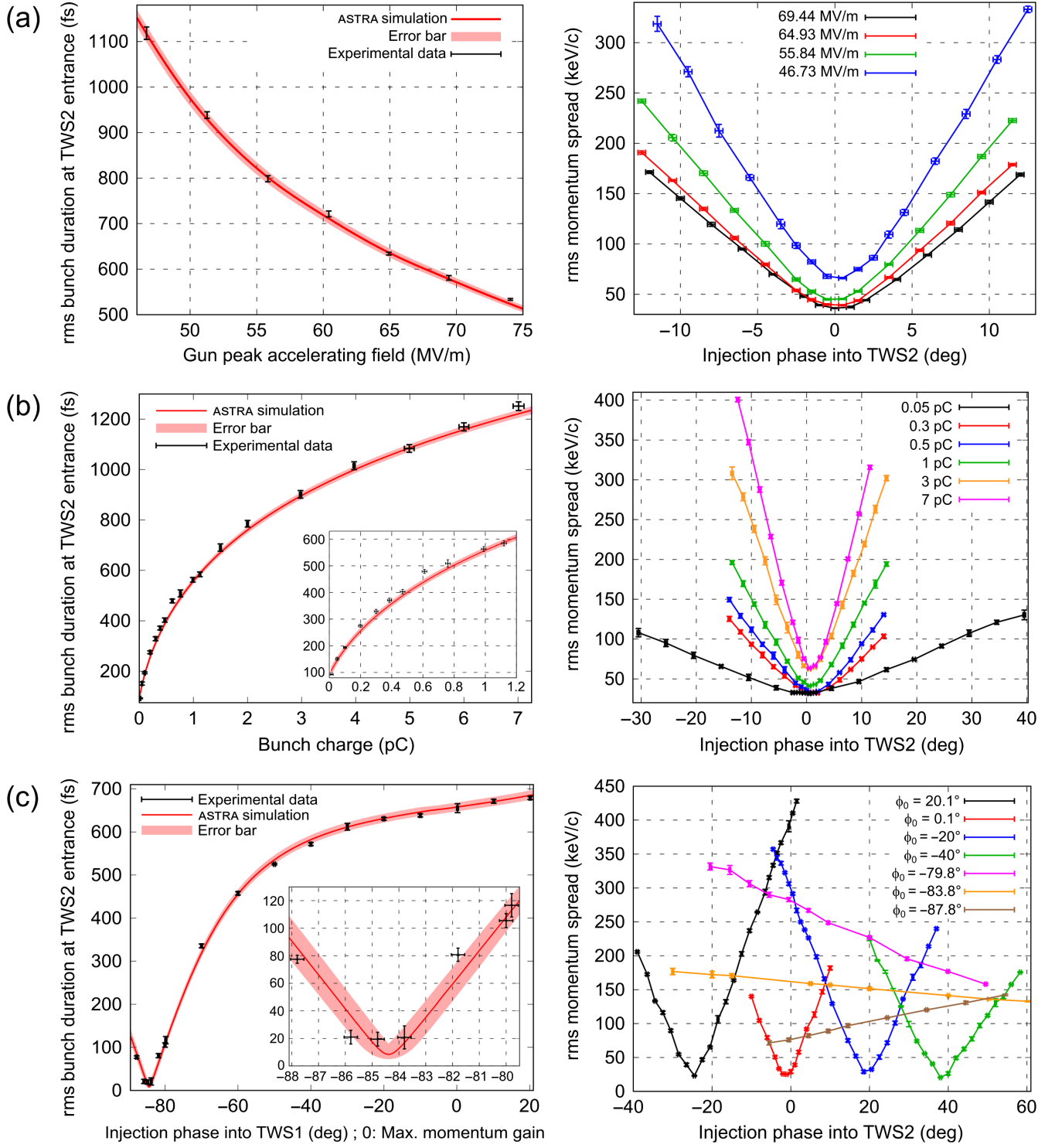


FIG. 9. rms bunch duration at TWS2 entrance as a function of the rf-gun peak accelerating field (a), the bunch charge (b) and the injection phase into TWS1 (c). $0^\circ \equiv$ maximum momentum gain. Aside of each duration curve, a selection of the raw data used for the measurements is displayed. Conditions: Mo (a,b) and Cs_2Te (c) cathode; $320\ \mu\text{m}$ (a,c) and $800\ \mu\text{m}$ (b) transverse diameter of laser pulse driving the rf gun; $64.9\ \text{MV/m}$ (b) and $69.5\ \text{MV/m}$ (c) gun peak accelerating field (respectively, 3.43 and $3.64\ \text{MeV/c}$ output momentum); $(1.08$ to $1.05 \pm 0.02)$ pC depending on point (a) and (1.27 ± 0.02) pC before collimator and (1.01 ± 0.02) pC after collimator (c); Injection phases into rf gun adjusted to maximize the momentum (except for the points at $46.7\ \text{MV/m}$ (respectively, $51.3\ \text{MV/m}$) in (a) where it is fixed to $+6.7^\circ$ (resp. $+11.7^\circ$) above the zero-crossing field); Injection phase into TWS1 adjusted to maximize the momentum gain (a,b); see Table II. Note: For (b), the error bars on the charge for the three highest points are larger because of a different setting of the Faraday cup. The charge for the lowest point ($0.015\ \text{pC}$) has not been directly measured with the Faraday cup but extrapolated from the cathode laser settings.

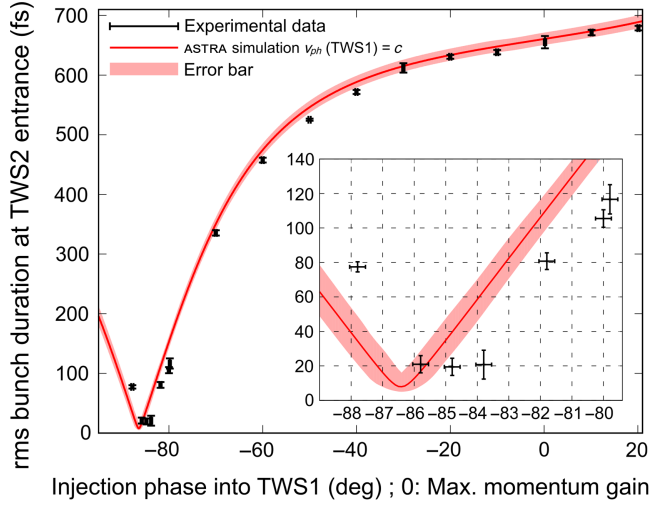


FIG. 10. rms bunch duration at TWS2 entrance as a function of the injection phase into TWS1 ($0^\circ \equiv$ maximum momentum gain). The phase velocity of TWS1 is here set to c (the design value) in the ASTRA simulation, instead of the experimentally measured value ($1.00040c$) as in Fig. 9(c). Conditions: See Fig. 9(c).

simulations instead of the default design value (c), we computed the distance between the edge of the error range of the experimental data and the edge of the error range of the simulated data. This distance is set to zero when the error regions are overlapping. The results as a function of the injection phase into TWS1 are shown in Table V, where they are normalized to the experimentally measured bunch duration and expressed in percent. A 0% value therefore means that the experimental data agree with the simulated ones within the error bars, not that they are equal. This is the case for both simulated dataset ($v_{ph}(\text{TWS1}) = 1.00040c$ and $v_{ph}(\text{TWS1}) = c$) for the injection phases into TWS1 ranging from $+20.1^\circ$ to -30° (the first six experimental data points in Fig. 9(c)). Table V therefore only displays the range from -40° to -87.8° , where differences appear.

From Table V, it is visible that the agreement between experimental data and simulations remains almost perfect when the experimentally measured TWS1 phase velocity ($1.00040c$) is used in the latter. Indeed, all the points overlap each other within their error bars, except at the injection phase into TWS1 of -70° where a minor disagreement exists. The behavior is clearly different when the default design value is used in simulations for TWS1 phase velocity (c). In fact, a limited disagreement appears in the injection phase region between -40° and -70° , which then generally significantly increases when approaching and overcoming the injection phase of maximal bunch compression. One can note that the agreement becomes better again for the injection phases of -84.8° and especially -85.8° . However, as clearly visible in Fig. 10, this is simply a coincidence due to the fact that the experimental data and simulation curves cross each other in this region.

TABLE V. Agreement between the experimentally measured bunch durations and the simulated ones presented in Fig. 9(c) when the experimentally measured $v_{ph}(\text{TWS1})$ ($1.00040c$) is used in simulations and in Fig. 10 when the design value (c) is used by default in simulations. $\phi_0(\text{TWS1})$: Injection phase into TWS1; $\sigma_{t_{\text{exp}}}$: Experimentally measured rms bunch duration; $\Delta\sigma_t(v_{ph} = 1.00040c)$ (resp. $\Delta\sigma_t(v_{ph} = c)$): Distance between the edge of the experimental data error box and the edge of the simulated data error channel when $v_{ph}(\text{TWS1}) = 1.00040c$ (resp. $v_{ph}(\text{TWS1}) = c$) is used in simulations (set to 0 when the error regions are overlapping). Conditions: See captions of Figs. 9(c) and 10.

$\phi_0(\text{TWS1})$	$\sigma_{t_{\text{exp}}}$	$\Delta\sigma_t(v_{ph}=1.00040c)$	$\Delta\sigma_t(v_{ph}=c)$
		$\sigma_{t_{\text{exp}}}$	$\sigma_{t_{\text{exp}}}$
-40°	571.8 ± 3.3 fs	0%	+0.69%
-50°	525.2 ± 1.8 fs	0%	+1.88%
-60°	457.5 ± 4.0 fs	0%	+0.70%
-70°	335.5 ± 4.4 fs	-0.30%	+0.09%
-79.8°	116.6 ± 8.5 fs	0%	+18.71%
-80°	105.5 ± 5.1 fs	0%	+30.04%
-81.8°	80.7 ± 4.8 fs	0%	+17.60%
-83.8°	20.7 ± 8.4 fs	0%	+104.46%
-84.8°	19.5 ± 5.0 fs	0%	+14.74%
-85.8°	21.0 ± 5.0 fs	0%	0%
-87.8°	77.4 ± 2.9 fs	0%	-32.92%

The combined analysis of Figs. 9(c), 10, and Table V clearly demonstrates that a precise experimental determination of the TWS phase velocity is required to properly simulate the velocity bunching process and subsequently obtain a reliable comparison with the experimental data.

In Figs. 9(a) and 9(b), we show only simulations with $v_{ph}(\text{TWS1}) = 1.00040c$ and do not compare with simulations where $v_{ph}(\text{TWS1}) = c$. This is due to the fact that the injection phase into TWS1 is set to 0° for these two figures. In this phase region, the difference between simulations with $v_{ph} = c$ and $v_{ph} = 1.00040c$ is small and well below the error bars so that no significant difference would be visible.

Figure 11 shows a close-up of Fig. 9(c) around the compression maximum, where a curve is superimposed to evaluate if the applicability criterion derived in Sec. III B is fulfilled. For this purpose, the variable $(\sigma_{p_{f_{\text{max}}}} - \sigma_{p_{f_{\text{min}}}})/(R\langle p \rangle)$ is used. As visible in Fig. 11, it is greater than 2 for all the experimental data, meaning that the theoretical applicability criterion from Sec. III B is fulfilled. It is not fulfilled only in a small range between -84.1° and -84.55° , where no experimental data have been acquired. However, it is also visible that for the experimental data at -83.8° and -84.8° , the variable $(\sigma_{p_{f_{\text{max}}}} - \sigma_{p_{f_{\text{min}}}})/(R\langle p \rangle)$ is only around 5. As explained in Sec. III B, this tends to increase the uncertainty of the phase-scan method, because only a small number of data points can then be used as input for the phase-scan method. This is especially visible

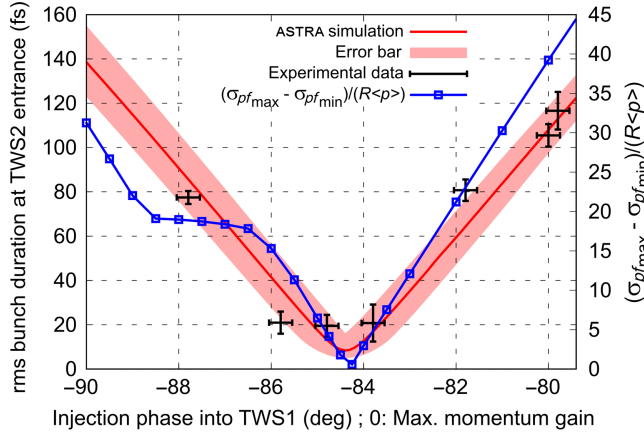


FIG. 11. rms bunch duration at TWS2 entrance and $(\sigma_{pf_{\max}} - \sigma_{pf_{\min}})/(R\langle p \rangle)$ as a function of the injection phase into TWS1 ($0^\circ \equiv$ maximum momentum gain). The variable $(\sigma_{pf_{\max}} - \sigma_{pf_{\min}})/(R\langle p \rangle)$ is used to check the applicability of the phase-scan method (see Sec. III B). Conditions: See Fig. 9(c).

for the point at -83.8° where the uncertainty on the retrieved bunch duration approaches 50%.

One can also remark in Fig. 11 that the three points at -83.8° , -84.8° and -85.8° do not follow the shape of the simulation curve and are rather aligned along a flat line around 20 fs rms, which is a sign of a practical resolution limit of the phase-scan method under the ARES operation conditions.

To understand this resolution limit and investigate its cause, we simulated the bunch duration measurement with ASTRA. Namely, we simulated the bunch momentum spread at the high-energy spectrometer as a function of the injection phase into TWS2 for several injection phases into TWS1 around the maximal compression (at -84.3° in simulations). For these simulations, we restricted the range of simulated injection phases into TWS2 to the one we used in our experiments. We then applied the model presented in Sec. III A to the simulated datasets and compared the reconstructed bunch duration $\sigma_{t_{\text{reconstr}}}$ to the input one of the simulation (at TWS2 entrance) $\sigma_{t_{\text{init}}}$, which is the target of the reconstruction. The results are shown in Table VI.

One can see in Table VI that $\sigma_{t_{\text{reconstr}}}$ also exhibits a resolution limit (around 15 fs rms) in the vicinity of the point of maximal compression, and the shortest values of $\sigma_{t_{\text{init}}}$ cannot be reconstructed accurately. This resolution limit does not come from the number of momentum spread values as a function of the injection phase into TWS2 used to compute $\sigma_{t_{\text{reconstr}}}$. In fact, this number is not limited in simulations, contrary to our experimental measurements where it is limited by the resolution of the high-energy spectrometer. The observed resolution limit for $\sigma_{t_{\text{reconstr}}}$ is therefore induced by other experimental conditions. As explained at the end of Sec. III B, two effects becoming not negligible for short bunches come into play, namely,

TABLE VI. Reconstructed bunch duration at TWS2 entrance ($\sigma_{t_{\text{reconstr}}}$) as a function of the injection phase into TWS1 [ϕ_0 (TWS1)]. $\sigma_{t_{\text{reconstr}}}$ is obtained by applying the model presented in Sec. III A to simulated curves of bunch momentum spread at the high-energy spectrometer as a function of the injection phase into TWS2. $\sigma_{t_{\text{init}}}$ is the simulated bunch duration at TWS2 entrance and therefore the target of the reconstruction. Conditions: See Fig. 9(c).

ϕ_0 (TWS1)	$\sigma_{t_{\text{init}}}$	$\sigma_{t_{\text{reconstr}}}$
-82.8°	40.0 fs	37.2 fs
-83.2°	30.5 fs	27.2 fs
-83.5°	23.5 fs	19.4 fs
-83.8°	16.8 fs	15.7 fs
-84°	12.8 fs	15.3 fs
-84.2°	9.6 fs	15.3 fs
-84.5°	8.8 fs	17.1 fs
-84.8°	13.3 fs	19.9 fs
-85.2°	22.1 fs	25.2 fs
-85.5°	29.2 fs	31.9 fs

the change of the bunch momentum spread between TWS2 entrance and the high-energy spectrometer induced by the space-charge forces and the not constant duration of the bunch throughout TWS2. These two effects affect the reconstructed bunch duration and are therefore likely responsible for the experimental resolution limit observed in Fig. 9(c).

One can observe that the experimental resolution limit from Fig. 9(c) (≈ 20 fs rms) is slightly higher compared to the simulated one from Table VI (≈ 15 fs rms). This difference can be explained by the fact that the experimental measurements are limited by the high-energy spectrometer resolution, while the simulations are not. It could also be explained by a difference in the space-charge forces intensity between experiments and simulations, which could, for example, come from a different bunch transverse profile evolution into TWS2.

The minimum experimentally measured bunch duration of 20 fs rms is, to the best of our knowledge, around 4 times shorter than what has been previously experimentally demonstrated based on rf-phasing techniques with a single rf structure [23]. It could be slightly improved, within the limits of the applicability criterion discussed in Sec. III B, by reducing the space-charge forces effect. This could be achieved by reducing the bunch charge and/or the distance between TWS2 and the high-energy spectrometer. In general, but not applicable to ARES, using several TWS would also improve the resolution by inducing more momentum spread variation.

VI. CONCLUSION AND OUTLOOK

The commissioning phase leading to the first characterization of the duration of the electron bunches generated by the ARES linac at DESY has been presented. An rf-phasing technique, the phase-scan method, has been

applied with a 4.092 m long S-band traveling wave accelerating structure for this purpose.

The sensitivity of the method allowed highlighting different response times for the Mo and Cs₂Te cathodes mounted in the ARES rf gun, the value of around 270 fs for the Cs₂Te cathode estimated from comparison with ASTRA simulations being consistent with direct measurements reported in the literature.

The overall very good agreement between the experimental measurements and the predictions from ASTRA simulations demonstrates that the ARES operation is well understood on the bunch duration aspect for a large range of operation parameters (charge, gun peak field, and injection phase into TWS1). An important requirement for that is the preliminary determination of the phase velocity in TWS1. To this aim, we proposed a simple beam-based method precise down to a variation of one part per ten thousand respective to c . This method is of particular interest for the facilities aiming to generate short electron bunches through the velocity bunching process since the phase velocity has a major influence on it. It is applicable to any accelerator at the condition that a not ultrarelativistic beam (typically ≤ 5 MeV/ c) of precisely known momentum (uncertainty better than a few percent) can be delivered at the entrance of a TWS and a downstream momentum measurement is available.

The shortest bunch duration measured on ARES with the phase-scan method after compression via velocity bunching in TWS1 is around 20 fs rms, which is very likely limited by the influence of the space-charge forces. This represents the first experimental demonstration of the ARES linac ability to generate ultrashort electron bunches. It is, therefore, a strong basis for future demonstrations toward the ARES objective of even shorter bunches (fs to sub-fs scale), which will require a dedicated diagnostic to be resolved. The first PolariX-TDS [31–33] is expected to be commissioned at ARES in the first half of 2024, and the second one in the second half of 2024 at the earliest, to fulfill this purpose. The phase-scan method, now routinely used at ARES, will be an important benchmark tool during the commissioning phase of the PolariX-TDS and will also continue to serve as additional diagnostics thereafter.

The capability of ARES to generate ultrashort electron bunches in the range of around 100 MeV combined with the availability of conventional diagnostics will be of primary importance for the TWAC project [47], which aims to develop THz-driven structures for the purpose of acceleration and compression of electron bunches down to tens of fs rms. The ARES linac will serve as a test bench for the development of advanced compact duration diagnostics within the framework of this project.

ACKNOWLEDGMENTS

The authors acknowledge support from DESY (Hamburg, Germany), a member of the Helmholtz

Association HGF. The authors would like to thank the technical groups at DESY for the installation, development, and regular maintenance of the ARES linac. The authors also thank U. Dorda and B. Marchetti for their leading work during the installation, conditioning, and early commissioning phases of the ARES linac. The authors thank K. Flöttmann for his careful reading of the manuscript and his suggestions to improve it. Funding has been received from the European Union's Horizon Europe research and innovation program (EIC Pathfinder) under Grant agreement No. 101046504. Views and opinions expressed are those of the authors only and do not necessarily reflect those of the European Union or EISMEA. Neither the European Union nor the granting authority can be held responsible for them.

-
- [1] W. Helml, I. Grguras, P. N. Juranić, S. Düsterer, T. Mazza, A. R. Maier, N. Hartmann, M. Ilchen, G. Hartmann, L. Patthey, C. Callegari, J. T. Costello, M. Meyer, R. N. Coffee, A. L. Cavalieri, and R. Kienberger, Ultrashort free-electron laser X-ray pulses, *Appl. Sci.* **7**, 915 (2017).
 - [2] K. Floettmann, F. Lemery, M. Dohlus, M. Marx, V. Tsakanov, and M. Ivanyan, Superradiant cherenkov-wakefield radiation as THz source for FEL facilities, *J. Synchrotron Radiat.* **28**, 18 (2021).
 - [3] D. Filippetto, P. Musumeci, R. K. Li, B. J. Siwick, M. R. Otto, M. Centurion, and J. P. F. Nunes, Ultrafast electron diffraction: Visualizing dynamic states of matter, *Rev. Mod. Phys.* **94**, 045004 (2022).
 - [4] W. E. King, G. H. Campbell, A. Frank, B. Reed, J. F. Schmerge, B. J. Siwick, B. C. Stuart, and P. M. Weber, Ultrafast electron microscopy in materials science, biology and chemistry, *J. Appl. Phys.* **97**, 111101 (2005).
 - [5] J. Yang, T. Kondoh, K. Kan, and Y. Yoshida, Ultrafast pulse radiolysis, *Nucl. Instrum. Methods Phys. Res., Sect. A* **629**, 6 (2011).
 - [6] E. Panofski, R. Assmann, F. Burkart, U. Dorda, L. Genovese, F. Jafarinia, S. Jaster-Merz, M. Kellermeier, W. Kuropka, F. Lemery, B. Marchetti, D. Marx, F. Mayet, T. Vinatier, and S. Yamin, Commissioning results and electron beam characterization with the s-band photo-injector at SINBAD-ARES, *Instruments* **5**, 28 (2021).
 - [7] F. Burkart, R. W. Assmann, H. Dinter, S. Jaster-Merz, W. Kuropka, F. Mayet, B. Stacey, and T. Vinatier, The ARES Linac at DESY, in *Proceedings of the 31st International Linear Accelerator Conference (LINAC'22)*, Liverpool, United Kingdom, 2022 (JACoW, Geneva, Switzerland, 2022), THPOJO01, pp. 691–694.
 - [8] S. Jaster-Merz, R. W. Assmann, R. Brinkmann, F. Burkart, and T. Vinatier, First studies of 5D phase-space tomography of electron beams at ARES, in *Proceedings of the 31st International Linear Accelerator Conference, LINAC'22*, Liverpool, United Kingdom, 2022, (JACoW, Geneva, Switzerland, 2022), MOPORI10, pp. 247–251.
 - [9] TWAC website, <https://twac.ijclab.in2p3.fr/en/twac/> (2023).

- [10] F. Mayet, R. Assmann, J. Bödwadt, R. Brinkmann, U. Dorda, W. Kuroepka, C. Lechner, B. Marchetti, and J. Zhu, Simulations and plans for possible DLA experiments at SINBAD, *Nucl. Instrum. Methods Phys. Res., Sect. A* **909**, 213 (2018).
- [11] J. Valdmánis, G. Mourou, and C. Gabel, Picosecond electro-optic sampling system, *Appl. Phys. Lett.* **41**, 211 (1982).
- [12] I. Wilke, A. M. MacLeod, W. A. Gillespie, G. Berden, G. M. H. Knippels, and A. F. G. van der Meer, Single-shot electron-beam bunch length measurements, *Phys. Rev. Lett.* **88**, 124801 (2002).
- [13] E. Roussel, C. Szwarz, C. Evain, B. Steffen, C. Gerth, B. Jalali, and S. Bielawski, Phase diversity electro-optic sampling: A new approach to single-shot terahertz waveform recording, *Light Sci. Appl.* **11**, 14 (2022).
- [14] P. Heil, K. Aulenbacher, C. Matejcek, S. Friederich, M. Bruker, and F. Fichtner, Coherent Smith-Purcell radiation for minimally invasive bunch length measurement at the subpicosecond time scale, *Phys. Rev. Accel. Beams* **24**, 042803 (2021).
- [15] I. Nozawa, K. Kan, J. Yang, A. Ogata, T. Kondoh, M. Gohdo, K. Norizawa, H. Kobayashi, H. Shibata, S. Gonda, and Y. Yoshida, Measurement of < 20 fs bunch length using coherent transition radiation, *Phys. Rev. ST Accel. Beams* **17**, 072803 (2014).
- [16] I. Nozawa, M. Gohdo, K. Kan, T. Kondoh, A. Ogata, J. Yang, and Y. Yoshida, Bunch length measurement of femtosecond electron beam by monitoring coherent transition radiation, in *Proceedings of the 6th International Particle Accelerator Conference (IPAC'15)*, Richmond, VA, 2015 (JACoW, Geneva, Switzerland, 2015), MOPTY002, pp. 940–943.
- [17] Q. Q. Su, J. F. Hua, Z. Nie, Y. Ma, S. Liu, Y. F. Zheng, C.-H. Pai, and W. Lu, Temporal diagnostics of femtosecond electron bunches with complex structures using sparsity-based algorithm, *Phys. Rev. Accel. Beams* **21**, 112801 (2018).
- [18] P. Emma, J. Frisch, and P. Krejcik, A transverse RF deflecting structure for bunch length and phase space diagnostics, LCLS Technical Note No. 12, 2000.
- [19] M. Röhrs, C. Gerth, H. Schlarb, B. Schmidt, and P. Schmüser, Time-resolved electron beam phase space tomography at a soft x-ray free-electron laser, *Phys. Rev. ST Accel. Beams* **12**, 050704 (2009).
- [20] C. Behrens, F. Decker, Y. Ding, V. A. Dolgashev, J. Frisch, Z. Huang, P. Krejcik, H. Loos, A. Lutman, T. J. Maxwell, J. Turner, J. Wang, M. Wang, J. Welch, and J. Wu, Few-femtosecond time-resolved measurements of X-ray free-electron lasers, *Nat. Commun.* **5**, 3762 (2014).
- [21] L. Zhao, Z. Wang, C. Lu, R. Wang, C. Hu, P. Wang, J. Qi, T. Jiang, S. Liu, Z. Ma, F. Qi, P. Zhu, Y. Cheng, Z. Shi, Y. Shi, W. Song, X. Zhu, J. Shi, Y. Wang, L. Yan, L. Zhu, D. Xiang, and J. Zhang, Terahertz streaking of few-femtosecond relativistic electron beams, *Phys. Rev. X* **8**, 021061 (2018).
- [22] G. Andonian, E. Hemsing, D. Xiang, P. Musumeci, A. Murokh, S. Tochitsky, and J. B. Rosenzweig, Longitudinal profile diagnostic scheme with subfemtosecond resolution for high-brightness electron beams, *Phys. Rev. ST Accel. Beams* **14**, 072802 (2011).
- [23] D. X. Wang, G. A. Krafft, and C. K. Sinclair, Measurement of femtosecond electron bunches using a rf zero-phasing method, *Phys. Rev. E* **57**, 2283 (1998).
- [24] T. Vinatier, C. Bruni, S. Chancé, and P. Puzo, Length measurement of high brightness electron beam thanks to the 3-phase method, in *Proceedings of the 5th International Particle Accelerator Conference, IPAC-2014, Dresden, Germany* (JACoW, Geneva, Switzerland, 2014), pp. 3459–3461.
- [25] T. Vinatier, Influence of laser parameters on the relativistic short electron bunches dynamics in linear accelerators based on RF-guns and development of associated diagnostics, Ph.D. thesis, Laboratoire de l'Accélérateur Linéaire, Université Paris Sud, Orsay, France, 2015, pp. 95–110.
- [26] T. N. Hu, Y. J. Pei, and G. Y. Feng, Bunch length evaluation for typical low-energy beam injectors based on RF-phasing techniques, *Nucl. Instrum. Methods Phys. Res., Sect. A* **916**, 87 (2019).
- [27] D. H. Dowell, P. R. Bolton, J. E. Clendenin, S. M. Gierman, C. G. Limborg, B. F. Murphy, J. F. Schmerge, and T. Shaftan, Longitudinal emittance measurements at the SLAC gun test facility, *Nucl. Instrum. Methods Phys. Res., Sect. A* **507**, 331 (2003).
- [28] J. Hwang, T. Miyajima, Y. Honda, and E. Kim, Measurement of bunch length and temporal distribution using accelerating radio frequency cavity in low-emittance injector, *Sci. Rep.* **10**, 18905 (2020).
- [29] D. Malyutin, M. Gross, I. Isaev, M. Khojayan, G. Kourkafas, M. Krasilnikov, B. Marchetti, M. Otevrel, F. Stephan, and G. Vashchenko, Longitudinal phase space tomography using a booster cavity at PITZ, *Nucl. Instrum. Methods Phys. Res., Sect. A* **871**, 105 (2017).
- [30] H. Loos, P. R. Bolton, J. E. Clendenin, D. H. Dowell, S. M. Gierman, C. G. Limborg, J. F. Schmerge, T. V. Shaftan, and B. Sheehy, Longitudinal phase space tomography at the SLAC gun test facility and the BNL DUV-FEL, *Nucl. Instrum. Methods Phys. Res., Sect. A* **528**, 189 (2004).
- [31] P. Craievich *et al.*, Novel X-band transverse deflection structure with variable polarization, *Phys. Rev. Accel. Beams* **23**, 112001 (2020).
- [32] B. Marchetti *et al.*, Experimental demonstration of novel beam characterization using a polarizable X-band transverse deflection structure, *Sci. Rep.* **11**, 3560 (2021).
- [33] D. Marx, R. W. Assmann, P. Craievich, K. Floettmann, A. Grudiev, and B. Marchetti, Simulation studies for characterizing ultrashort bunches using novel polarizable X-band transverse deflection structures, *Sci. Rep.* **9**, 19912 (2019).
- [34] K. Flöttmann, Astra: A space-charge tracking algorithm, <https://www.desy.de/mpyflo/>, DESY, Hamburg, Germany.
- [35] B. Marchetti, R. Assmann, C. Behrens, R. Brinkmann, U. Dorda, K. Floettmann, I. Hartl, M. Huening, Y. Nie, H. Schlarb, and J. Zhu, Electron-beam manipulation techniques in the SINBAD linac for external injection in plasma wake-field acceleration, *Nucl. Instrum. Methods Phys. Res., Sect. A* **829**, 278 (2016).
- [36] L. Serafini and M. Ferrario, Velocity bunching in photoinjectors, *AIP Conf. Proc.* **581**, 87 (2001).

- [37] W. Kuropka, R. W. Assmann, F. Burkart, H. Dinter, S. Jaster-Merz, F. Lemery, F. Mayet, B. Stacey, and T. Vinatier, Commissioning of a movable bunch compressor for sub-fs electron bunches, in *Proceedings of the 31st International Linear Accelerator Conference, LINAC'22, Liverpool, United Kingdom, 2022* (JACoW, Geneva, Switzerland, 2022), THPOJO02, pp. 695–698.
- [38] J. Zhu, R. W. Assmann, M. Dohlus, U. Dorda, and B. Marchetti, Sub-fs electron bunch generation with sub-10-fs bunch arrival-time jitter via bunch slicing in a magnetic chicane, *Phys. Rev. Accel. Beams* **19**, 054401 (2016).
- [39] M. Ferrario, M. Migliorati, and L. Palumbo, Space charge effects, in *Proceedings of the CAS-CERN Accelerator School: Advanced Accelerator Physics, Trondheim, Norway, 2013*, CERN-2014-009 (CERN, Geneva, 2014), edited by W. Herr, pp. 331–356.
- [40] F. Mayet, M. Hachmann, K. Floettmann, F. Burkart, H. Dinter, W. Kuropka, T. Vinatier, and R. Assmann, Predicting the transverse emittance of space charge dominated beams using the phase advance scan technique and a fully connected neural network, *Phys. Rev. Accel. Beams* **25**, 094601 (2022).
- [41] H. Wiedemann, *Particle Accelerator Physics* (Springer, Nature, 2015).
- [42] R. L. Harrison, Introduction to Monte Carlo simulation, *AIP Conf. Proc.* **1204**, 17 (2010).
- [43] A. Aryshev, M. Shevelev, Y. Honda, N. Terunuma, and J. Urakawa, Femtosecond response time measurements of a Cs₂Te photocathode, *Appl. Phys. Lett.* **111**, 033508 (2017).
- [44] G. Loisch, Y. Chen, C. Koschitzki, H. Qian, M. Gross, A. Hannah, A. Hoffmann, D. Kalantaryan, M. Krasilnikov, S. Lederer, X. Li, O. Lishilin, D. Melkumyan, L. Monaco, R. Niemczyk, A. Oppelt, D. Sertore, F. Stephan, R. Valizadeh, G. Vashchenko, and T. Weibach, Direct measurement of photocathode time response in a high-brightness photo-injector, *Appl. Phys. Lett.* **120**, 104102 (2022).
- [45] R. H. Fowler and L. Nordheim, Electron emission in intense electric fields, *Proc. R. Soc. A* **119**, 173 (1928).
- [46] D. Lipka, J. Lund-Nielsen, and M. Seebach, Resonator for charge measurement at REGAE, in *Proceedings of the 2nd International Beam Instrumentation Conference, IBIC-2013, Oxford, United Kingdom, 2013* (JACoW Publishing, Geneva, Switzerland, 2013), WEPF25, pp. 872–875.
- [47] C. Bruni *et al.*, TWAC: EIC Pathfinder open European project on novel dielectric acceleration, in *Proceedings of the 14th International Particle Accelerator Conference, IPAC-2023, Venezia, Italy* (JACoW, Geneva, Switzerland, 2013), TUPA061, pp. 1450–1453.